coatings

MDPI

Article

Microstructure and Tribological Performance of TiB_2-NiCr Composite Coating Deposited by APS

Ning Zhang [1], Nannan Zhang [1,*], Xufeng Wei [2], Yue Zhang [1] and Deyuan Li [1]

[1] Department of Material Science and Engineering, Shenyang University of Technology, Shenyang 110870, China; zhangning201610034@sut.edu.cn (N.Z.); yuezhang@sut.edu.cn (Y.Z.); dmy1962@sut.edu.cn (D.L.)
[2] Dalian Huarui Heavy Industrial Special Spare Parts Co., Ltd., Dalian 116052, China; weixf@dhidcw.com
* Correspondence: zhangnn@sut.edu.cn; Tel.: +86-24-2549-6812

Academic Editor: Robert B. Heimann
Received: 19 October 2017; Accepted: 18 December 2017; Published: 20 December 2017

Abstract: Nickel chromium (NiCr) powders with different titanium diboride (TiB_2) additions (20, 40 and 60 wt %) were prepared with a mechanical alloying method and then sprayed using an air plasma spraying technology. The microstructure and phase composite of the powders and the cross-sections of deposited coatings were analyzed with a scanning electronic microscope and X-ray diffraction. The tribological performance of the coatings was studied using a pin-on-disk tribometer at room temperature. The weight loss of the as-sprayed coating was measured by using a high accuracy weighing balance. Cr_3C_2-25NiCr coating was produced and tested for comparison. The morphologies of the worn surface were then investigated. Parts of debris with some scratches were found, presenting typical signs of abrasive wear and showing slight adhesive wear on the surface. The 20 wt % additive TiB_2 coating demonstrated the highest microhardness and the lowest coefficient of friction. The wear resistance of the metal-ceramic composites coatings was enhanced with the addition of TiB_2.

Keywords: TiB_2-NiCr; air plasma spray; mechanical alloying; tribological property

1. Introduction

Automobile brakes are the most pivotal and demanding component in the automobile safety system [1]. According to statistics, 30% of automobile accidents in the country are caused by brake failure, and poor quality brake pads are the main cause of failure. Semi-metal friction materials, such as steel fibers, are widely used in China as brake pads [2]. A new material is needed since the steel fibers may cause brake shrinkage and brake fluid boiling when the temperature increases. Thermal sprayed cermet coatings on the running surface of the brake pads have been considered as an alternative method to solve this problem [3,4].

As a potential boride ceramic material, pure titanium diboride (TiB_2) has some excellent properties such as high hardness (34 GPa), a high melting point (2980 °C), a higher Young's modulus (414 GPa at 1090 °C) and a lower friction coefficient compared to Fe [5,6]. Therefore, an increasing number of studies have focused on producing TiB_2-based ceramic coatings [7–10]. Wang et al. [11] cladded TiB_2 and TiC powders on an AISI 1045 steel surface and found that the wear resistance was improved in dry sliding conditions. Dallaire et al. [12] tried to create flux-cored wires composed of 304 stainless steel shells filled with additive of 10–65 wt % TiB_2 powders, which was then sprayed using the twin arc spraying method. James et al. [13] investigated the composition of Ni and TiB_2 coatings and sputtering operation parameters to protect substrates from solid particle erosion. However, limited research exists on the tribological performance of TiB_2 and NiCr coatings in thermal spraying.

Pure TiB_2 is brittle and easily reacts with oxygen at high temperature, so it should cohere to soft materials to form a metal-ceramic coating, such as NiCr alloy [14,15]. In this work, TiB_2 and NiCr

powders with different additions of TiB_2 (20, 40 and 60 wt %) were mixed using mechanical alloying (MA) and then sprayed using air plasma spraying (APS) technology. The effect of adding TiB_2 on the tribological performance of the coating was then investigated.

2. Experimental Procedure

The source material for the surface coating was a mixture of the $Ni_{80}Cr_{20}$ alloy powder (Ti Metal Materials Co., Ltd., Changsha, China) and TiB_2 powder (Xiangtian Nano Materials Co., Ltd., Shanghai, China) selected using a mesh size of 300, with the ratios of TiB_2 mass fraction of 20%, 40% and 60%. The two powders were mixed using the ball-milling method. The 304 stainless steel balls (ball-to-powder weight ratio of 15:1) were put into a planetary ball grinding mill (KQM-X/B, Xianyang Jinhong General Machinery Co., Ltd., Xianyang, China) and milled with a rotation speed of 300 r/min for 20 h. The powders were classified into three types: 20TiB_2-NiCr, 40TiB_2-NiCr and 60TiB_2-NiCr. Another commercial powder labeled Cr_3C_2-25NiCr (Praxair Co., Ltd., Danbury, CT, USA) was selected to prepare the coatings for comparison. The compositions of TiB_2, NiCr and Cr_3C_2-25NiCr powders are listed in Table 1.

Table 1. Compositions of the powders (wt %).

Materials	Ti	B	Fe	Co	Mn	C	N	O	Cr	Si	Ni
TiB_2	Bal.	30.75	0.14	0.011	0.03	0.13	0.2	0.5	–	–	–
NiCr	–	–	–	–	–	0.01	–	0.025	19.86	0.02	Bal
Cr_3C_2-25NiCr	–	–	–	–	–	10	–	–	Bal.	0	20

These powders were deposited on Q235 steel substrate (80 mm × 30 mm × 30 mm) by using the SG-100DC plasma torch (Praxair 3710, Praxair, Cleveland, OH, USA). The plasma spray parameters are shown in Table 2. The plasma flux was obtained by a mixture of argon (Ar) and helium (H_2) to melt a mass of particles using the relatively high temperature inside the anode. The current intensity was maintained at 600 A, and the H_2 flow rate was 10 L/min, which supplied the heat. Before plasma spraying, these substrate surfaces were sand blasted using Al_2O_3 sand with a mesh size of 30, followed by de-greasing using acetone. When the coatings were sprayed, the samples were cut into small cross-sections for metallography.

Table 2. Plasma spraying operation parameters.

Parameters	Value
Current (A)	600
Voltage (V)	40
Ar/H_2 (L/min)	40/10
Powder feed rate (g/min)	30–40
Gun traverse speed (mm/s)	100
Spraying distance (mm)	100
Pre-heating temperature (°C)	150

The morphologies of the powder and cross-sections samples were observed using a scanning electron microscope (SEM, S-3400N, Hitachi, Tokyo, Japan) equipped with an energy dispersive spectrometer (EDS). In addition, the phase composition of the powders and coatings was characterized using X-ray diffraction (XRD, Shimadzu 7000, Shimadzu, Kyoto, Japan) using monochromatic Cu-Kα radiation (λ = 0.1541 nm) at 40 kV, 30 mA. The Vickers microhardness tester (HVS-1000, TMTeck Instrument Co., Ltd., Beijing, China) was used to measure the coating hardness, with 200g force for 15 s.

To simulate the wear between the friction blocks of the brake pads and the brake disc, gray iron was used as the counterpart [16,17]. The friction tests were performed using an MM-W1 abrasion

tester (Jinan Hensgrand Instrument Co., Ltd., Jinan, China) with 100 N loading and 100 r/min during the process.

3. Results and Discussion

3.1. Characterization of Powders

Images of the three different contents of the TiB_2-NiCr powders after ball-milling and Cr_3C_2-25NiCr powders are shown in Figure 1. An enlarged picture is inserted in the top-left for observing the morphology of a single particle. The 20TiB_2-NiCr powder is nearly rounded and it has better liquidity for spraying. The NiCr powders were crushed and adhered to the TiB_2 powder surface after a long ball milling. The TiB_2-NiCr particle is significantly different from the Cr_3C_2-25NiCr particle, which has a hollow structure, as shown in Figure 1d.

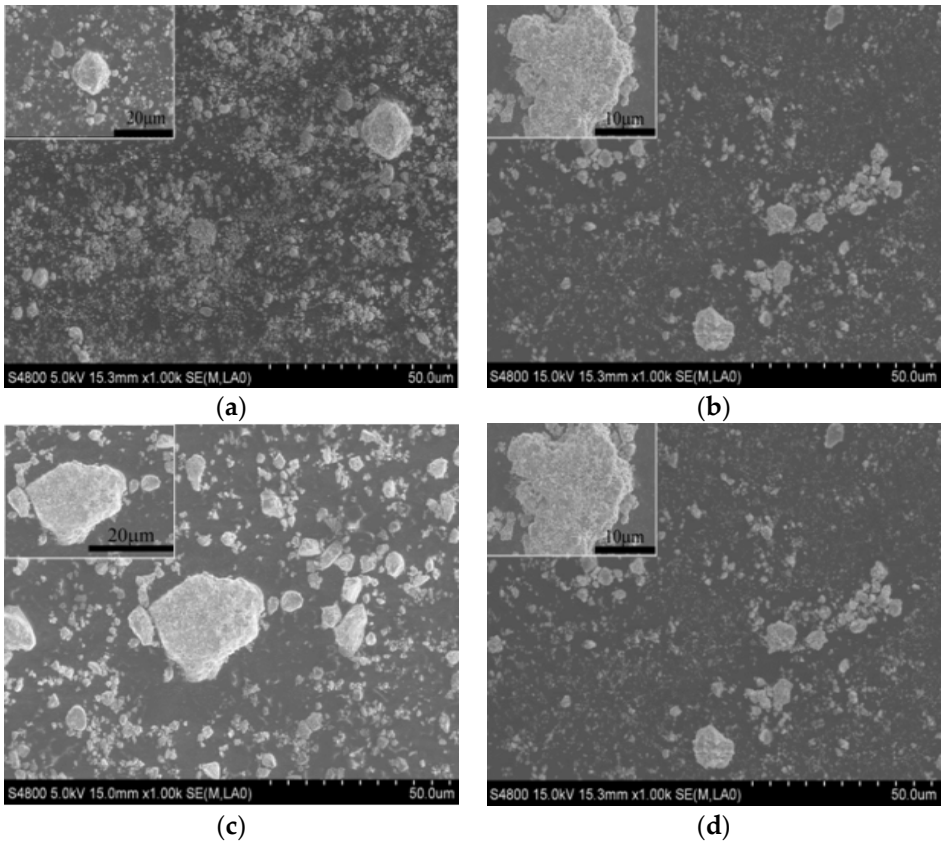

Figure 1. Morphology of the powder after the mechanical alloying (MA): (**a**) 20TiB_2-NiCr; (**b**) 40%TiB_2-NiCr; (**c**) 60TiB_2-NiCr; and (**d**) Cr_3C_2-25NiCr.

Figure 2 shows the XRD analysis results for the three TiB_2-NiCr powders. The Ni and TiB_2 accounted for the majority of the phases of the powders, having a small CrB phase. However, hardly any NiCr phases were detected in the XRD spectrum. During the long time of milling, Ni could react with TiB_2 to form brittle borides and liberate Ti. The mechanical energy was transformed to heat energy, which could provide enough energy for these reactions. These reactions can spontaneously occur through the calculated standard Gibbs free energy [18]. The chemical equation that occurred in the MA is as follows:

$$TiB_2 = Ti + 2B \quad (1)$$

$$NiCr + B = Ni + CrB \quad (2)$$

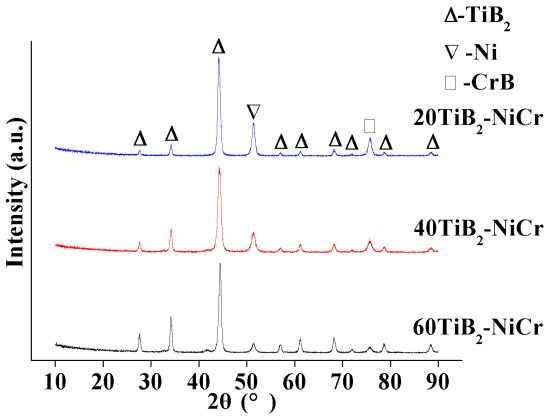

Figure 2. X-ray diffraction (XRD) spectrum of three TiB_2-NiCr powders.

3.2. Coating Morphology and Phase Composition

The cross-section morphologies of 20TiB_2-NiCr, 40TiB_2-NiCr, 60TiB_2-NiCr and Cr_3C_2-25NiCr coatings are shown in Figure 3. The coatings present a typical and dense lamellar structure [19]. The dark semi-molten or molten TiB_2 particles with different shapes are not uniformly distributed in the lamellas. The reason for this phenomenon is that TiB_2 has a higher melting point, at approximately 3000 °C, and strongly resists plastic deformation even at high temperatures [8]. The ceramic phase in metal ceramic coatings has anti-solid particles or abrasive wear resistance, and the metallic phase protects the ceramic phase from breaking off. Based on the energy spectrum data in Table 3, the three-phase microstructure is clearly seen in Figure 3a. The black-colored circular Zone A is TiB_2, which plays a major role in improving the wear resistance of the materials. The irregular light gray Zone B is mainly Cr_2O_3, which is mainly composed of the oxidation phases in the coating. The remaining grey Zone C is the NiCr bonding phase. However, some gray areas are dissolved Ti and O elements. The deeper the gray scale, the lower the dissolved Ti and O elements.

The distribution of defects is delineated by the large black irregular area, called Zone D (Figure 3b), where the ceramic phase has broken off, and the small black round areas are the pores. In the process of spraying, when these molten particles impact the sprayed coating, a liquid–solid transformation of spray particles occurred due to rapid cooling. The volume shrinkage between the interlayer produced these pores. For these individual particles, the ceramic particles deposited their local heat to the sprayed layer, also forming some closed pores. The microstructure of 60TiB_2-NiCr is similar to the other TiB_2-NiCr coatings, and the chemical compositions in Zones E and F are found in Table 3.

We found that the 20 wt % TiB_2-NiCr coating had a higher deposition rate of about 88%. The most probable reason for this finding is that the additive TiB_2 particles decreased the adherence of the interface [20]. A number of TiB_2 particles hit the substrate and bounced into the air during the plasma spray process, leading to TiB_2 loss. When the mass fraction of TiB_2 reached 60%, the coating was the thinnest at nearly 90 μm, as shown in Figure 3c. Notably, amounts of boride loss can lead to tissue redistribution in cermet coating, called a boride-free path (indicated as λ: the distance from the adjacent boride), which affects the coating mechanical properties.

The two-phase microstructure is clearly shown in Figure 3d, including the light-colored NiCr phase (Zone G) and the gray matrix Cr_3C_2 phase (Zone H). For the NiCr binding phase, different levels of gray represent different levels of dissolved Cr and C elements. The deeper the gray scale, the higher the dissolved Cr and C elements. When the in-flight particles are in the high temperature plasma jet, because the NiCr metal binding phase coated the carbide surface and the binder phase has a lower melting point (1415 °C) compared to carbide (>1500 °C), the binding phase is molten and dissolves near carbide. A similar situation occurs between the NiCr phase and boride. The NiCr binding phase is molten and dissolves near boride.

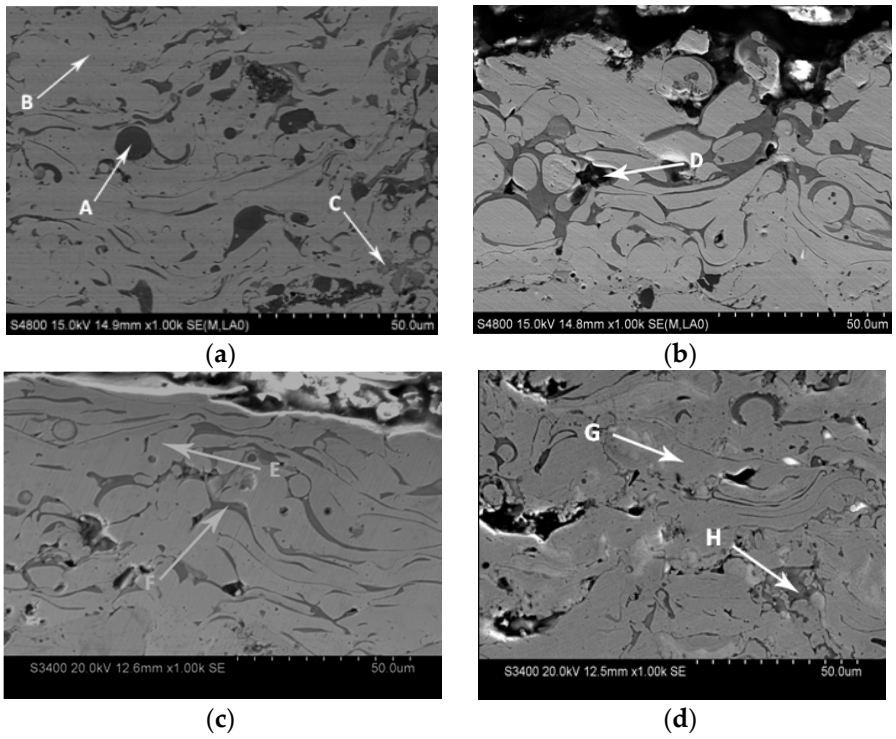

Figure 3. Microstructure of the coating: (**a**) 20TiB_2-NiCr; (**b**) 40TiB_2-NiCr; (**c**) 60TiB_2-NiCr; and (**d**) Cr_3C_2-25NiCr.

Table 3. The chemical composition (at.%) in different regions.

Figure 3	Zone	Ni	Cr	C	O	Ti	B
(a)	A	0.60	–	–	–	38.78	60.62
	B	26.09	11.54	–	59.28	3.09	–
	C	78.62	19.98	–	–	1.40	–
(c)	E	73.70	12.87	–	–	1.16	12.26
	F	12.97	26.65	–	25.28	25.26	9.86
(d)	G	72.38	14.62	11.11	1.89	–	–
	H	1.23	55.10	43.67	–	–	–

The XRD analysis results performed on the TiB_2-NiCr coatings are shown in Figure 4. Some new phases occurred, and the Ni phase disappeared compared to the powders. This occurred because, during the spraying process, the Ni first reacted with B as a protective layer to reduce the reaction between O_2 and TiB_2. However, some other phases were still present in the coatings. In Figure 3b, the black belt around the binding phase is Cr_2O_3, with a small amount of TiO_2 and B_2O_3. This is produced by the oxidation reaction between Cr in the binding phase and a small amount of boride with O_2 in the spraying process. Cr mainly occurs during oxidation; Ni and B are generated from the chemical reaction, forming BNi_2 and Ni_4B_3, which are related to the reaction thermodynamics. The oxygen pressure for metal oxide is higher than the decompression pressure of oxide, since the decompression pressure of Cr_2O_3 (1000 °C, 10^{-8} MPa) is far lower than the decompression pressure of NiO (1000 °C, 10^{-4} MPa), so the Cr_2O_3 phase is mostly generated. However, when the oxidation of boride occurred, hardly any B_2O_3 was produced. During the spraying process, the oxidation and dissolution of boride will decrease in the mechanical properties of the coatings.

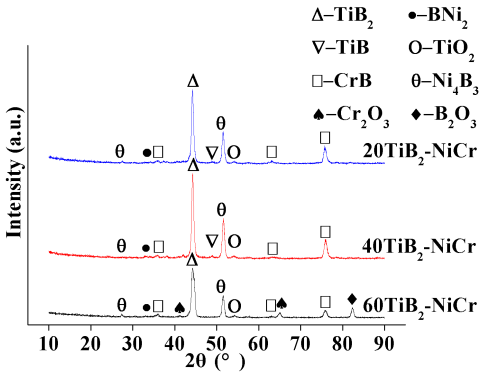

Figure 4. The XRD spectrum of three TiB_2-NiCr coatings.

Figure 5 shows the microhardness curve of three TiB_2-NiCr coatings and a Cr_3C_2-25NiCr coating from substrate to top coating. The average hardness value of the 20 wt % TiB_2-NiCr coating was 818 HV, with a maximum value of 850 HV. The increase in hardness is attributed to the heterogeneous distribution of TiB_2 particles. The 40 wt % and 60 wt % TiB_2 coatings had average hardness values of about 684 HV and 569 HV, respectively. For the Cr_3C_2-25NiCr coating, the average hardness was about 427 HV, which was lower than all the TiB_2-NiCr coatings. The TiB_2 phase strengthening effect and Cr_3C_2 decomposition during the spraying process were responsible for this effect. The higher levels of NiCr binder phase (20 wt % TiB_2-NiCr) not only increased the coating deposition rate, they maintained TiB_2 particles in this coating to help increase the coating microhardness.

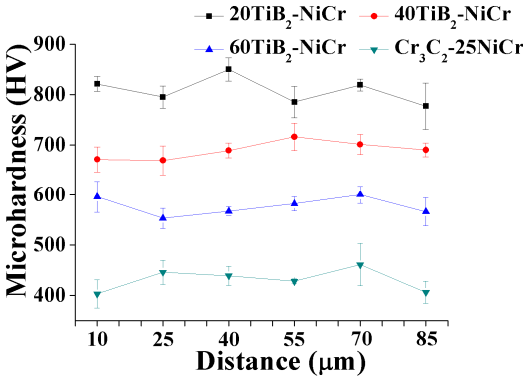

Figure 5. Microhardness of TiB_2-NiCr and Cr_3C_2-25NiCr coating.

3.3. Tribological Performance of Coatings

Figure 6 shows the friction coefficient curve of the TiB_2-NiCr and Cr_3C_2-25NiCr coatings. The friction coefficient attained a steady state approximately at five minutes of run time. The trend in average friction coefficient as a function of TiB_2 content was mainly similar to that of hardness. The friction coefficient reached a minimum value at 20 wt % TiB_2. The friction coefficient of Cr_3C_2-25NiCr was higher than all the TiB_2-NiCr coatings. TiB_2 is naturally chemically inert, meaning it has a low equilibrium solubility with Fe [21]; hence, finding adhesive wear in a dense TiB_2-phase is difficult.

Figure 7 shows the mass loss of all the coatings after sliding wear testing. The trend in mass loss was similar to that of the friction coefficient. With the addition of the 20 wt % TiB_2, the mass loss was 0.00023 g, which was the best wear resistance. The mass loss of the Cr_3C_2-25NiCr coating was significantly higher than the others, at nearly six-times higher than the 20TiB_2-NiCr coating. At 400 °C, TiB_2-NiCr coatings may form more B_2O_3 phase, which plays an important role in self-lubrication to reduce the mass loss of the surface during the wear process.

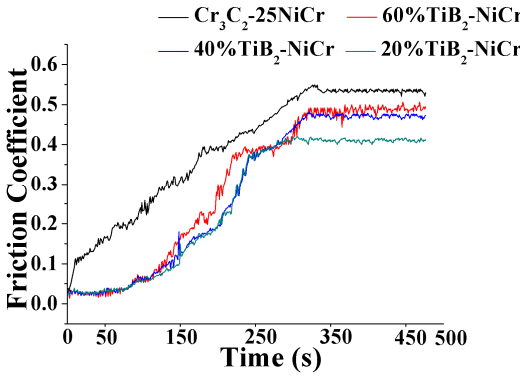

Figure 6. Coefficient of friction of coatings.

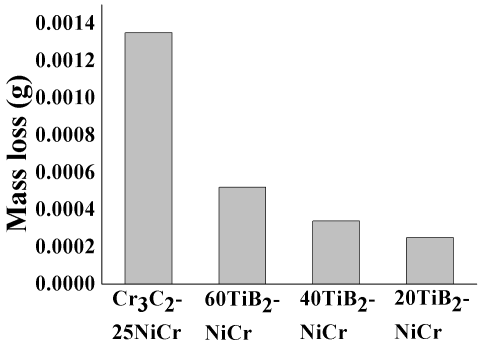

Figure 7. Mass loss of TiB_2-NiCr and Cr_3C_2-25NiCr coatings.

By observing the surface after wear, the wear process for these coatings could be analyzed, as shown in Figure 8. Figure 8a shows the worn surface of the 20 wt % TiB_2-NiCr coating, which had the highest hardness. Some debris and some grooves are present, which are typical characteristics of abrasive wear with slight adhesive wear. The hard phase, which mostly included M_xB_y such as TiB_2, TiB, CrB, and Ni_4B_3 from the XRD results, became some new sources of wear. With increasing the additive TiB_2, the grooves gradually disappeared, and some transfer layers appeared. As seen in Figure 8a, the wear process generated a considerable amount of plate-like debris. With the decrease in hardness, abrasive wear will not occur; the wear mechanism changes from abrasive wear to adhesive wear. Compared to the TiB_2-NiCr coating, some small cracks were observed on the Cr_3C_2-25NiCr coating's worn surface. Once these cracks cause the hard phases to fall off, abrasive particles may be produced that lead to three-body wear. Therefore, the mass loss of the Cr_3C_2-25NiCr coating was the greatest.

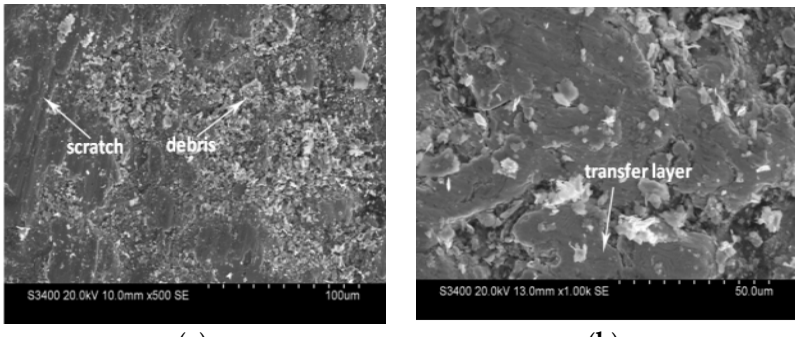

(**a**) (**b**)

Figure 8. *Cont.*

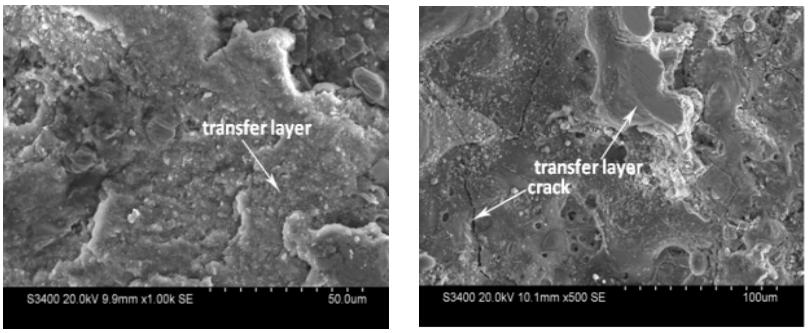

(**c**) (**d**)

Figure 8. Worn surface of a pin: (**a**) 20TiB_2-NiCr; (**b**) 40TiB_2-NiCr; (**c**) 60TiB_2-NiCr; and (**d**) Cr_3C_2-25NiCr.

4. Conclusions

In this work, TiB_2-NiCr and Cr_3C_2-25NiCr coatings were deposited by using atmosphere plasma spray. Based on the analysis of the microstructure and wear resistance of these coatings, we drew the following conclusions.

- The TiB_2-NiCr coatings had a typical dense lamellar structure. The as-sprayed coating contained mainly TiB_2, Ni_4B_3 and CrB phases.
- The TiB_2-NiCr coatings showed higher hardness, lower mass loss and a lower friction coefficient than the Cr_3C_2-25NiCr coating.
- With the continuous increase in TiB_2 content, the hardness and wear resistance decreased due to the TiB_2 deposition rate. The 20 wt % TiB_2-NiCr coating demonstrated the best wear resistance.
- The wear resistance changed from abrasive wear to adhesive wear when the 40 wt % and 60 wt % TiB_2 were added.

Acknowledgments: This work was financially supported by the Natural Science Foundation of Liaoning Province (No. 201602553) and the Chinese National Natural Science Foundation (No. 51301112).

Author Contributions: Ning Zhang performed the experiments and wrote the manuscript. Nannan Zhang conceived of and designed the experiments. Xufeng Wei assisted in SEM analysis. Yue Zhang analyzed the XRD data. Deyuan Li proofread the grammar.

Conflicts of Interest: The authors declare no conflict of interest.

References

1. Hou, Z.X.; Jin, Q. Preparation and property study of composite cermet coating used in automobile brake shoes. *Therm. Spray Technol.* **2012**, *4*, 46–60. [CrossRef]
2. Yang, Y.; Liu, B.W.; Xiong, X. Study on friction and wear properties of a new ceramic-based automotive braking pads. *Powder Metall. Technol.* **2010**, *28*, 336–341. [CrossRef]
3. Kermc, M.; Kalin, M.; Vizintin, J. Development and use of an apparatus for tribological evaluation of ceramic-based brake materials. *Wear* **2005**, *259*, 1079–1087. [CrossRef]
4. Ambrosio, E.P.; Pavese, M.; Biamino, S.; Epicoco, P.; Tulliani, J.M.; Fossati, P.; Marino, F.; Fino, P. Cost effective glassy carbon brake pad solution for automotive systems. *Adv. Appl. Ceram.* **2012**, *111*, 427–432. [CrossRef]
5. Wu, Y.; Zeng, D.; Liu, Z.; Qiu, X.; Zhong, X.; Yu, H.; Li, S. Microstructure and sliding wear behavior of nanostructured Ni60-TiB_2 composite coating sprayed by HVOF technique. *Surf. Coat. Technol.* **2011**, *206*, 1102–1108. [CrossRef]
6. Wang, H.; Li, H.; Zhu, H.; Cheng, F.; Wang, D.; Li, Z. A comparative study of plasma sprayed TiB_2-NiCr and Cr_3C_2-NiCr composite coatings. *Mater. Lett.* **2015**, *153*, 110–113. [CrossRef]
7. Yan, H.; Zhang, P.; Yu, Z.; Lu, Q.; Yang, S.; Li, C. Microstructure and tribological properties of laser-clad Ni-Cr/TiB_2 composite coatings on copper with the addition of CaF_2. *Surf. Coat. Technol.* **2012**, *206*, 4046–4053. [CrossRef]

8. Zhu, H.; Li, H.; Li, Z. Plasma sprayed TiB_2-Ni cermet coatings: Effect of feedstock characteristics on the microstructure and tribological performance. *Surf. Coat. Technol.* **2013**, *235*, 620–627. [CrossRef]
9. Umanskyi, O.; Hussainova, I.; Storozhenko, M.; Terentyev, O.; Antonov, M. Effect of oxidation on sliding wear behavior of NiCrSiB-TiB_2 plasma sprayed coatings. *Key Eng. Mater.* **2014**, *604*, 16–19. [CrossRef]
10. Zhang, M.; Qu, K.L.; Luo, S.X.; Liu, S.S. Effect of Cr on the microstructure and properties of TiC-TiB_2 particles reinforced Fe-based composite coatings. *Surf. Coat. Technol.* **2017**, *316*, 131–137. [CrossRef]
11. Wang, X.; Pan, X.; Du, B.; Li, S. Production of in situ TiB_2 + TiC/Fe composite coating from precursor containing B_4C-TiO_2-Al powders by laser cladding. *Trans. Nonferr. Met. Soc. China* **2013**, *23*, 1689–1693. [CrossRef]
12. Dallaire, S.; Levert, H. Development of cored wires for improving the abrasion wear resistance of austenitic stainless steel. *J. Therm. Spray Technol.* **1997**, *6*, 456–462. [CrossRef]
13. Wert, J.J.; Oppliger, S.J. The influence of composition and processing parameters on the mechanical properties and erosion response of Ni-TiB_2 coatings. *J. Mater. Eng. Perform.* **1992**, *1*, 129–142. [CrossRef]
14. Yue, X.; Cai, Z.; Lu, X.; Wang, J.; Ru, H. Effect of Ni content on microstructures and mechanical properties of hot-pressed TiC-TiB_2-Ni composite. *Mater. Sci. Eng. A* **2016**, *668*, 208–214. [CrossRef]
15. Jones, M.; Horlock, A.J.; Shipway, P.H.; Mccartney, D.G.; Wood, J.V. A comparison of the abrasive wear behavior of HVOF sprayed titanium carbide-and titanium boride-based cermet coatings. *Wear* **2001**, *251*, 1009–1016. [CrossRef]
16. Gigan, G.; Ekh, M.; Vernersson, T.; Lunden, R. Modelling of grey cast iron foe application to brake discs for heavy vehicles. *Proc. Inst. Mech. Eng. Part D J. Automob. Eng.* **2017**, *231*, 35–49. [CrossRef]
17. Cho, M.H.; Kim, S.J.; Basch, R.H.; Fash, J.W.; Jang, H. Tribological study of gray cast iron with automotive brake linings: The effect of rotor microstructure. *Tribol. Int.* **2003**, *36*, 537–545. [CrossRef]
18. Li, J.; Zhang, X.J.; Wang, H.P.; Li, M.P. Microstructure and mechanical properties of Ni-based composite coatings reinforced by insitu synthesized TiB_2 + TiC by laser cladding. *Int. J. Miner. Metall. Mater.* **2013**, *20*, 57–64. [CrossRef]
19. Zhang, N.; Lin, D.; He, B.; Zhang, G.; Li, D. Effect of oxyacetylene flame remelting on wear behaviour of supersonic air-plasma sprayed NiCrBSi/h-BN composite coatings. *Surf. Rev. Lett.* **2017**, *24*, 83–90. [CrossRef]
20. Zhu, H.; Li, H. Tribological Performance of TiB_2-Ni Composite Coating Deposited by APS. *Rare Met. Mater. Eng.* **2012**, *41*, 481–486.
21. Vleugels, J.; Kumar, K.C.H.; Vitchev, R.G.; Vanderbiest, O. Unlubricated fretting wear of TiB_2-containing composites against bearing steel. *Metall. Mater. Trans. A* **2002**, *33*, 3847–3859. [CrossRef]